2022 IEEE 61st Conference on Decision and Control (CDC)
December 6-9, 2022. Cancún, Mexico

Task-Invariant Centroidal Momentum Shaping for Lower-Limb Exoskeletons

Miao Yu, Student Member, *IEEE* and Ge Lv, Member, *IEEE*

2022 IEEE 61st Conference on Decision and Control (CDC) | 978-1-6654-6761-2/22/$31.00 ©2022 IEEE | DOI: 10.1109/CDC51059.2022.9993080

***Abstract*— Task-invariant approaches are desirable in exoskeleton control design as they have the potential of providing consistent assistance across locomotor tasks. Different from traditional trajectory-tracking approaches that are specific to tasks and users, task-invariant control approaches do not replicate normative joint kinematics, which could eliminate the need for task detection and allow more flexibility for human users. In this paper, we propose a task-invariant control paradigm for lower-limb exoskeletons to alter the human user's centroidal momentum, i.e., a sum of projected limb momenta onto the human's center of mass. We design a virtual reference model based on human user's self-selected gaits to provide a reference centroidal momentum for the exoskeleton to track and make it adaptable to changes in gait patterns. Mathematically, the proposed approach reduces the control design problem into a lower-dimensional space. With the number of actuators being greater than the dimension of the centroidal momentum vector, we can guarantee the existence of a centroidal momentum shaping law for underactuated systems through optimization. Simulation results on a human-like biped show that the proposed shaping strategy can produce beneficial results on assisting human locomotion, such as metabolic cost reduction.**

I. INTRODUCTION

People with afflictions such as muscle weakness suffer from decreasing walking speed, partial or complete movement impairment and therefore limit their societal participation [1]. Traditional assistive devices such as mobile walkers, body-weight support systems are often used for assisting human locomotion [2]. However, there exist critical drawbacks for these devices that limit their overall adaptability. For instance, conventional body-weight support systems can offload a human user's weight during walking [3], but they can only be used in clinical environments. Similarly, mobile walkers [4] can provide balance support for their users during walking. However, they require constant grasping by the user and are not equipped with joint-level actuators, therefore are not able to provide specific assistance for impaired limbs. Emerging powered lower-limb exoskeletons have demonstrated great potential in assisting human locomotion. Equipped with actuators, they can inject active energy into the human-exoskeleton system to compensate for the missing functions of impaired limbs [5], offload weights of extra loads [6], or reduce the human user's energy expenditure [7].

Exoskeleton control paradigms can be roughly divided into two categories: trajectory-based and trajectory-free approaches [8]. Trajectory-based control paradigms [9] track predefined kinematic trajectories, which does not encourage active user participation [8] nor promote user-friendly human-exoskeleton interaction [10] as individual's gaits are confined to specific patterns. Although some control paradigms are trajectory-free, they are specifically designed for dedicated tasks such as sit-to-stand [11] or stair ascent [12], where the proposed control methods cannot be easily translated into other locomotor tasks. Moreover, detecting transitions between tasks can be challenging in practice, which requires either computationally intensive switching algorithms [13] or manual inputs [14] from the users.

As the alternative category, trajectory-free approaches do not confine user's kinematics to specific gait patterns, therefore could allow users to select their own preferred gaits while being assisted by the exoskeletons. As one example, human muscle activation can be measured via Electromyography (EMG) sensors and used as real-time sensory feedback for control design to assist a weak person's lower-limb motion or improve the accuracy of human-machine interface [15]. However, performance of EMG sensors is suspectable to measurement noises, placement of electrodes, and sweating [8]. Energy shaping methods [16], [17] enable exoskeletons to provide task-invariant assistance by reducing the user's perceived body weight. Similarly, Lin et al. proposed a velocity-dependent energetic control method to provide task-invariant assistance by altering the closed-loop Hamiltonian [18]. While these approaches demonstrate promising results, solving the matching condition for high-dimensional underactuated systems is very difficult, especially with varying degrees of underactuation during different phases of gait. Thomas et al. proposed an energy shaping method to amplify human strength by virtually attaching a leg floating to the side of the true leg and obtaining the energy amplification ratio by changing the mass of the virtual leg [19]. While this control approach does not require the solving of matching conditions, it requires predefined joint positions of the virtual leg and thus may constrain the human user's movements.

An important metric used in bipedal locomotion control and evaluation is the centroidal momentum (CM), which is defined as the sum of projected segmental momenta onto the biped's center of mass (CoM) [20]. As a fixed dimensional, velocity-based vector, CM has been widely applied in locomotion associated design problems. For example, it can be used as an index for evaluating human walking stability with exoskeletons [21] and predicting human balance [22]. Similarly, horizontal and vertical momenta at the user's CoM can be used for trajectory planning in assisting sit-to-stand motion [23]. In addition, CM can be used for controlling

This work is supported by the South Carolina Translational Research Improving Musculoskeletal Health Faculty Development Award.

The authors are with the Department of Mechanical Engineering, Clemson University, Clemson, SC 29634 USA (e-mail: myu2@clemson.edu; glv@clemson.edu) (*Corresponding author: Ge Lv)*

walking patterns of humanoid or quadrupeds. Koolen et al. proposed a momentum-based control approach for humanoid robots to realize robust walking gaits [24]. Liu et al. used pre-planned future foot positions to calculate the desired CM for realizing quadrupedal trotting gaits [25]. The fact that the CM is a fixed-dimensional vector in 3D space regardless of biped models and the associated walking gaits brings several benefits for control design. As long as the number of exoskeleton actuators exceeds the CM's dimension, we can guarantee the existence of a control law to alter CM's direction or magnitude even if the system is underactuated. Control allocation (i.e., achieving a desired CM with specific actuators) can also be achieved, which is usually feasible when the system is overactuated [26]. Finally, altering the CM via exoskeleton actuators does not require knowledge of predefined reference trajectories, which may promote flexibility in control design and facilitate friendly human-exoskeleton interaction.

In this paper, we propose a task-invariant CM shaping framework for lower-limb exoskeletons. The shaping law is yielded through tracking the desired CM of a virtual reference model, whose joint positions and velocities are based on the human user's self-selected gaits. The inertial parameters of this model can be chosen as a scaled version of the human user's real mass and inertia, which will lead to a desired CM that has smaller or larger magnitudes. Through tracking this CM, we can mimic the behaviors of the virtual reference model via exoskeleton actuators to reduce/increase the perceived weight of the human user (see Fig. 1). Since the desired CM is generated based on each individual's self-selected gaits instead of predefined trajectories, and definition of CM does not restrict individual limb momentum, the proposed shaping framework is task-invariant. Instead of treating human torque inputs as noises, we use a nonlinear disturbance observer (NDO) to estimate volitional human joint torques and include them in the overall CM shaping design.

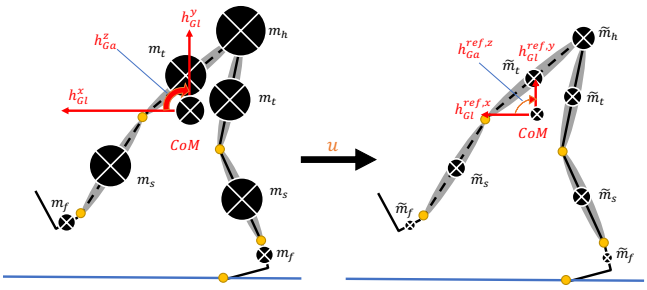

Fig. 1. Concept of shaping a human's CM (h_G, left) into a reference CM (h_G^{ref}, right) that has smaller magnitude via exoskeleton actuators. Subscripts l and a indicate the linear and angular components of the CM, respectively. This is a conceptual illustration, the actual CoM would be closer to the hip.

The rest of the paper is organized as follows: we begin in Sec. II by introducing the dynamics of the biped. In Sec. III, we define the reference CM based on the virtual reference model and derive the task-invariant CM shaping law. Simulation results and stability analysis using Poincaré sections are provided in Sec. IV. Finally, we draw conclusions and discuss possible future research directions in Sec. V.

II. DYNAMICS OF THE BIPED

Since human walking is primarily a sagittal-plane task [27], in this paper we assume the biped is ambulating in the sagittal plane and the inertial reference frame is defined at its heel or toe. Modeling the biped as a human wearing an exoskeleton, its Euler-Lagrange dynamics can be expressed as [28]

$$M\ddot{q}+C\dot{q}+N+A^T\lambda=\tau, \tag{1}$$

where $M\in\mathbb{R}^{n\times n}$ is the inertia matrix, $C\in\mathbb{R}^{n\times n}$ is the Coriolis/centrifugal matrix, $N\in\mathbb{R}^{n\times 1}$ denotes the gravitational forces, and n is the number of degrees of freedom (DoFs). Note that all the masses and inertia in these matrices are combinations of the human and exoskeleton parameters. The configuration vector is given as $q=(x,y,\phi,q_s^T)^T\in\mathbb{R}^2\times\mathbb{T}^{n-2}$, where x and y denote the Cartesian coordinates of the contact point, ϕ is the absolute angle defined with respect to the vertical axis, and $q_s\in\mathbb{T}^{n-3}$ is a vector composed of relative joint angles. Additionally, $\tau=\tau_{\text{hum}}+Bu$ denotes the sum of human joint torque vector τ_{hum} and the exoskeleton input Bu, where $B=(0_{p\times n-p},\ I_{p\times p})^T\in\mathbb{R}^{n\times p}$ is the matrix that maps the exoskeleton torque $u\in\mathbb{R}^p$ into the overall dynamics.

During a step, the biped's stance leg is always in contact with the ground. We can thus define proper holonomic contact constraints and map them into the overall dynamics via the constraint matrix A [28]. The term $\lambda=\hat{\lambda}+\check{\lambda}\tau$ in (1) denotes the ground reaction forces, which can be calculated using the method in [29]. Similar to [30], we assume the biped only has instantaneous double-support phase.

III. CENTROIDAL MOMENTUM SHAPING

While assisting the movement of individuals who have partial or full volitional control of their lower limbs, control strategies should be designed based on the individual's current motion and avoid relying on predefined trajectories. In this section, we propose a CM shaping strategy by leveraging the advantage of an autonomous reference model which has the same configuration as the human-exoskeleton model, but consists of a scaled version of human inertial parameters. The CM shaping law is yielded through tracking the desired CM generated by the reference model (see Fig. 2 for the overall structure of the control system).

A. Centroidal Momentum of the Biped

For any kinematic chain in 3D space, CM is always a vector in $\mathbb{R}^6$ [20]. The CM of a single-link robot can be expressed as $h_G=I_GV\in\mathbb{R}^6$, where $I_G=\text{diag}\{m,m,m,I,I,I\}$ is the inertia tensor with mass m and inertia I, and $V=[v^T,\omega^T]^T\in\mathbb{R}^6$ is the velocity vector with linear velocity $v\in\mathbb{R}^3$ and angular velocity $\omega\in\mathbb{R}^3$. To generalize this concept to a biped, which is a multi-link kinematic chain, we need to acquire the velocities of all links and project them onto the biped's CoM. The velocity vector of a biped v_G, which consists of velocities defined with respect to each link's body frame, is expressed as

$$v_G=J_G\dot{q},\quad J_G=[J_1^T,J_2^T,\cdots,J_j^T]^T, \tag{2}$$

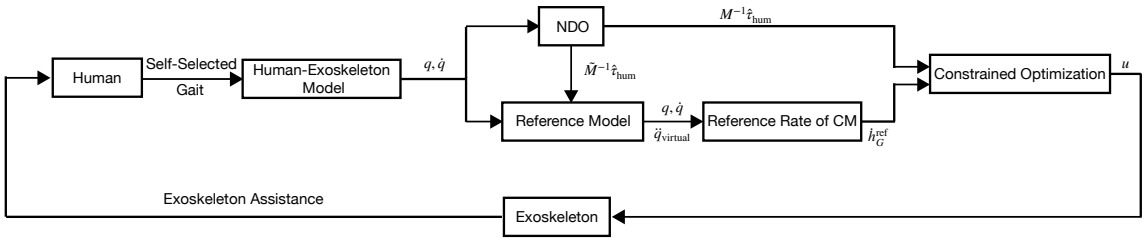

Fig. 2. Overall control diagram of CM shaping. The acronym NDO indicates "Nonlinear Disturbance Observer", which is used to estimate a modified form of human joint torques and will be specified in Sec. III-C.

where $J_G \in \mathbb{R}^{6\text{j}\times\text{n}}$ is the system Jacobian matrix composed of body Jacobian matrices $J_i \in \mathbb{R}^{6\times\text{n}}$, $i \in \{1,2,\cdots,\text{j}\}$ for all j links [28]. It follows that the body momentum vector $h_{\text{body}} \in \mathbb{R}^{6\text{j}}$ is given as

$$h_{\text{body}} = I_G v_G, \quad I_G = \text{diag}[I_{G1}, I_{G2}, \cdots, I_{Gj}], \tag{3}$$

where $I_G \in \mathbb{R}^{6\text{j}\times 6\text{j}}$ is the multi-link version inertia tensor composed of inertia tensor matrices $I_{Gi} \in \mathbb{R}^{6\times 6}$, $i \in \{1,2,3,\cdots,\text{j}\}$. Since we place body frames at the CoM of each link, I_{Gi} takes the form $I_{Gi} = \text{diag}[m_i \cdot I_{3\times 3},\ I_i \cdot I_{3\times 3}]$ with m_i and I_i being the mass and moment of inertia of link i, respectively. Finally, h_{body} is projected onto the biped's CoM to obtain the CM $h_G \in \mathbb{R}^6$ as

$$h_G = X_G^T h_{\text{body}}, \tag{4}$$

where $X_G \in \mathbb{R}^{6\text{j}\times 6}$ is the system adjoint transformation matrix. Summarizing (2) to (4), the CM of a multi-link biped can be expressed as

$$h_G = X_G^T I_G J_G \dot{q} := A_G \dot{q} \in \mathbb{R}^6, \tag{5}$$

where $A_G = X_G^T I_G J_G \in \mathbb{R}^{6\times\text{n}}$ is the centroidal momentum matrix.

Remark 1: By observing (5), h_G consists of two three-element parts, i.e., linear and angular momentum, respectively. With the assumption that the biped ambulates in the sagittal plane, the linear momentum along the z-axis and the angular momentum about the $x-$ and y-axes are zeros. As a result, only three rows in A_G are non-zero. Also, h_G is differentiable during each phase of a gait cycle [24], where $\dot{h}_G = A_G\ddot{q} + \dot{A}_G\dot{q}$.

B. Control Design

At this point, we are ready to derive the control law for shaping the CM. It is worth noting that our proposed control law is designed by tracking the desired CM of the reference model with desirable inertial parameters, whose angular information is extracted from the user's own preferred gaits, therefore is adaptable across locomotor tasks.

In order to design the shaping law, we will first need to define the reference CM h_G^{ref} and its derivative $\dot{h}_G^{\text{ref}}$. In this paper, we are particularly interested in the form

$$\dot{h}_G^{\text{ref}} = \dot{h}_G - K_p(h_G^{\text{ref}} - h_G), \tag{6}$$

where $K_p \in \mathbb{R}^{6\times 6}$ is a positive definite diagonal matrix. We proposed this relationship for h_G^{ref} and $\dot{h}_G^{\text{ref}}$ hoping that $\dot{h}_G$ will track $\dot{h}_G^{\text{ref}}$ while the difference between h_G and h_G^{ref} can be minimized via control actions. The reason that we prefer tracking the changing rate of h_G^{ref} rather than itself is that it will be generated only after the human starts walking. Similar to following a target vehicle with varying speeds, we hope to achieve the same velocity for the follower vehicle rather than a desired position over time.

Based on (5) and Remark 1, the reference CM and its derivative can thus be written as

$$h_G^{\text{ref}} = A_G^{\text{ref}}\dot{q}, \quad \dot{h}_G^{\text{ref}} = \dot{A}_G^{\text{ref}}\dot{q} + A_G^{\text{ref}}\ddot{q}_{\text{virtual}}, \tag{7}$$

where $\ddot{q}_{\text{virtual}}$ can be obtained from the desired dynamics of the virtual reference model

$$\tilde{M}\ddot{q}_{\text{virtual}} + \tilde{C}\dot{q} + \tilde{N} + A^T\tilde{\lambda} = \tau_{\text{hum}}. \tag{8}$$

In (8), τ_{hum} is the same human input vector as in (1), where its estimation method will be introduced in Sec. III-C. The matrices $\tilde{M}$, $\tilde{C}$, $\tilde{N}$, and $\tilde{\lambda}$ in (8) are defined similarly to the ones in (1) but with scaled inertial parameters, i.e., $m_i^{\text{ref}} = k_i m_i$, and $I_i^{\text{ref}} = k_i I_i$, where $k_i > 0$ is the scaling factor. Intuitively, $k_i > 1$ is denoted as resistive mode as the desired CM is defined with larger inertial parameters. On the contrary, $k_i < 1$ is denoted as assistive mode. Note that these reference matrices can have forms other than the ones with scaled inertial parameters, where alternative definitions will be investigated in future work.

Equating $\dot{h}_G$ in (6) with $A_G\ddot{q} + \dot{A}_G\dot{q}$ and plugging the expressions of h_G, h_G^{ref} and $\dot{h}_G^{\text{ref}}$ from (5) and (7), we can obtain

$$A_G\ddot{q} = \dot{A}_G^{\text{ref}}\dot{q} + A_G^{\text{ref}}\ddot{q}_{\text{virtual}} - \dot{A}_G\dot{q} + K_p(A_G^{\text{ref}}\dot{q} - A_G\dot{q}). \tag{9}$$

Substituting $\ddot{q}$ from (1) and plugging it into (9), we can obtain

$$\begin{aligned} A_G M^{-1} B_\lambda u = &-A_G M^{-1}(-C\dot{q} - N - A^T\hat{\lambda} + \tilde{\tau}_{\text{hum}}) \\ &- \dot{A}_G\dot{q} + \dot{A}_G^{\text{ref}}\dot{q} + A_G^{\text{ref}}\ddot{q}_{\text{virtual}} + K_p(A_G^{\text{ref}}\dot{q} - A_G\dot{q}), \end{aligned} \tag{10}$$

where $B_\lambda = B - A^T\check{\lambda}$ and $\tilde{\tau}_{\text{hum}} = (I - A^T\check{\lambda})\tau_{\text{hum}}$.

From Remark 1, A_G contains only three non-zero rows, therefore (10) can be reduced to three equivalent equations. If the number of exoskeleton actuators is more than three, then there exist infinite solutions to the control law u. We apply an optimization procedure with constraints to determine u as

$$\begin{aligned} \underset{u}{\text{Min}} \quad & u^T W u \\ \text{s.t.} \quad & A_G M^{-1} B_\lambda u = A_G M^{-1}(C\dot{q} + N + A^T\hat{\lambda} - \tilde{\tau}_{\text{hum}}) \end{aligned} \tag{11}$$

$$-\dot{A}_G\dot{q}+\dot{h}_G^{\text{ref}}+K_p(A_G^{\text{ref}}\dot{q}-A_G\dot{q}), \tag{12}$$
$$u_{\min}\le||u||_2\le u_{\max},$$

where $W\in\mathbb{R}^{\text{p}\times\text{p}}$ is a diagonal, semi-positive definite weight matrix, $u_{\min},\ u_{\max}\in\mathbb{R}$ are the lower and upper bounds of the control torques, respectively. The objective function is chosen as u^TWu to minimize the torques exerted by the exoskeleton actuators, which could possibly lead to an energy efficient solution. Additionally, the weight matrix W can be adjusted to achieve control allocation depending on specific assistive or resistive goals.

C. Nonlinear Disturbance Observer for Human Inputs

The proposed optimization procedure requires the knowledge of human input term τ_{hum}, which can be difficult to measure in practice. To overcome this issue, a nonlinear NDO can be applied to estimate human torques [31]. In this paper, we modify an existing NDO [31] so that it can estimate the modified form of human input $M^{-1}\tilde{\tau}_{\text{hum}}$ in (12) using joint parameters.

Multiplying M^{-1} from the left for (1), we can obtain

$$\ddot{q}+M^{-1}(C\dot{q}+N+A^T\hat{\lambda})=M^{-1}B_\lambda u+z, \tag{13}$$

where $z=M^{-1}\tilde{\tau}_{\text{hum}}$ denotes the "disturbance" to be observed. Re-writing (13) as

$$z=\ddot{q}+M^{-1}C\dot{q}+M^{-1}N+M^{-1}A^T\hat{\lambda}-M^{-1}B_\lambda u \tag{14}$$

and denoting the estimate of z as $\hat{z}$, we can obtain [32]:

$$\begin{aligned}\dot{\hat{z}}&=L(z-\hat{z}),\\&=-L\hat{z}+L[\ddot{q}+M^{-1}(C\dot{q}+N+A^T\hat{\lambda})-M^{-1}B_\lambda u]\end{aligned} \tag{15}$$

where $L\in\mathbb{R}^{\text{n}\times\text{n}}$ can be selected as a positive definite diagonal matrix so that the estimation error $e=z-\hat{z}$ is governed by

$$\dot{e}=\dot{z}-\dot{\hat{z}}=\dot{z}-Le. \tag{16}$$

If $\dot{z}$ is bounded, i.e., $||\dot{z}||_2\le\beta$ for some positive $\beta\in\mathbb{R}$, then the estimation error e is uniformly ultimately bounded by $2\beta\lambda_{\max}(P)/(\theta\lambda_{\max}(Q))$ [31], [32], where $\theta\in(0,1)$, P and Q are the associated positive definite matrices from the Lyapunov equation $PL+L^TP=Q$, and $\lambda_{\max}(\cdot)$ denotes the maximum eigenvalue of a matrix [32]. From [33], [34], we know that both τ_{hum} and M are bounded. In addition, we can numerically verify $\dot{M}^{-1}$ is also bounded based on the biped model, therefore $||\dot{z}||_2$ is bounded.

IV. SIMULATIONS AND RESULTS

In this section, we demonstrate potential benefits of the proposed CM shaping on human walking via simulations on an 8-DoF human-like biped.

A. Simulation Model and Hybrid Dynamics

The biped model we used for simulation is shown in Fig. 3, where its dynamics are in the form of (1). We lumped the human and the exoskeleton together to model the biped and assumed the biped's hip groups the human's torso and upper body masses. The biped's configuration vector is given as $q=\{\text{x},\text{y},\phi,\theta_{\text{a}},\theta_{\text{k}},\theta_{\text{h}},\theta_{\text{sk}},\theta_{\text{sa}}\}\in\mathbb{R}^2\times\mathbb{T}^6$, where $\theta_i,\ i\in\{\text{a},\text{k},\text{h},\text{sk},\text{sa}\}$ is the relative angle of ankle, knee, hip, swing knee, and swing ankle joints, respectively. Each of these joints is actuated by an exoskeleton actuator, i.e., $u=\{u_{\text{a}},u_{\text{k}},u_{\text{h}},u_{\text{sk}},u_{\text{sa}}\}\in\mathbb{R}^5$. Similarly, we define the human input vector as $\tau_{\text{hum}}=Bv$ with $v=\{v_{\text{a}},v_{\text{k}},v_{\text{h}},v_{\text{sk}},v_{\text{sa}}\}\in\mathbb{R}^5$. Each human joint torque is approximated by using a PD controller [29], i.e., $v_i=-K^v_{\text{pi}}(q_i-\bar{q}_i)-K^v_{\text{di}}\dot{q}_i$, where K^v_{pi} and K^v_{di} are semi-positive definite proportional and derivative gain matrices, and $\bar{q}_i$ is the equilibrium position of joint i. We first tuned the PD gains and the equilibrium positions by trial and error to find a stable passive gait walking down a shallow slope, and then implemented the shaping law u for simulations. All simulation parameters can be found in Table II of [29].

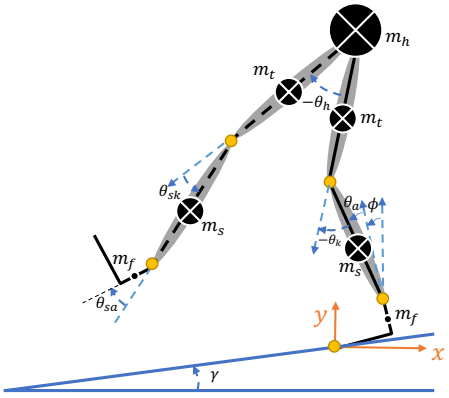

Fig. 3. Kinematic model of the human wearing an exoskeleton. The solid and dashed lines denote the stance and the swing leg, respectively. This figure is produced from [16].

Within a step, the biped goes through both the stance and swing phases, where the stance phase can be further divided into three contact phases: heel contact, flat foot, and toe contact. For each contact phase, we can define proper holonomic contact constraints and obtain a constant constraint matrix $A=[I_{c\times c},0_{c\times(n-c)}]$, where c represents the number of contact constraints. Transitions among these phases are modeled as discontinuous events, either an impact event or a change of coordinates, which leads to a hybrid dynamical system similar to the one in [35]. During simulation, we selected the reference model to have identical geometric shape as the human-exoskeleton model (i.e., Fig. 3) but with scaled inertial parameters to generate the reference CM.

B. Estimated Metabolic Cost Metrics

In order to verify if the proposed shaping strategy can reduce energy expenditure during walking, we compared the metabolic cost between passive gaits (i.e., $u=0$) and assisted/resisted walking with different combinations of K_p and k_i using two simulation-based metabolic cost metrics, where the first one [36] is expressed as

$$E_{\text{walking1}}=\frac{\int_0^T\tau_{\text{hum}}^2\,dt}{T(mgl)^2}\approx\frac{\sum_{i=1}^{N_T}\tau_{\text{hum}}^2(i)\Delta t(i)}{T(mgl)^2}. \tag{17}$$

In (17), T is the step duration, N_T is the number of timesteps during one step, m is the total mass of the biped, l is the

leg length, and $\Delta t(i)$ is the i-th timestep. Note that E_{walking1} is a unitless index. The second metric that we used can be expressed as [37]

$$E_{\text{walking2}} = (E_{\text{3LP}} + E_{\text{CR}} + E_{\text{GC}})/\eta + E_{\text{WS}}, \tag{18}$$

$$E_{\text{3LP}} = \int_0^T [\frac{d}{dt}(\frac{1}{2}\dot{q}^T M \dot{q})]^+ dt,$$

$$E_{\text{CR}} = \frac{1}{2} M v_z^2, \quad E_{\text{GC}} = 2 m_{\text{leg}} \Delta h_l g,$$

$$E_{\text{WS}} = \int_0^T m_{\text{leg}} g \cos\beta_s l_t \sin\frac{\theta_k}{2} \dot{\theta}_{\text{kmax}} \Phi(\frac{\dot{\theta}_k}{\dot{\theta}_{\text{kmax}}})\, dt,$$

where E_{3LP} is the swing and torso balance cost of the three-link (stance, swing leg, and torso) linear pendulum model, E_{CR} is the CoM redirection cost, E_{GC} denotes the ground clearance cost, and E_{WS} represents the weight support cost. Detailed definitions for all terms in (18) can be found in [37].

C. Results and Discussion

During simulation, we fixed the weight matrix W to be an identity matrix $I_{5\times5}$ and selected different combinations of K_p and k_i to study their effects on walking. In particular, we chose the same value for all diagonal elements for K_p. Note that the passive biped model is sensitive to system parameters when walking down the slope, which could fall over with K_p and/or k_i that are too small or too large. We therefore first varied these parameters to find their stable ranges as $k_i \in (0.85,\ 1.05)$ and $K_{\text{pi}} \in (10,\ 20)$. Humans will have better capacity to maintain balance and control of their bodies during walking compared to the passive biped, which could allow for a wider range for k_i and K_p.

We first examined the CM trajectories for different K_p and k_i combinations, where Fig. 4 shows the linear CM of the human-exoskeleton model along x-axis with three pairs of k_i and $K_p = 10 \cdot I_{6\times6}$ during 10 steps. CM along other axes are similar and have much smaller magnitudes, therefore are not demonstrated. In Fig. 4 we can see that modifying k_i results in noticeable changes in the magnitude of CM, while its general shape is preserved to passive walking, i.e., the proposed shaping law does not drastically interfere with the biped's walking pattern. All three CM curves converge within 8 steps.

Fig. 5 compares the reference CM and linear CM of the human-exoskeleton model along x-axis during one steady step with $k_i = 1.05$ and $K_p = 10 \cdot I_{6\times6}$. From this figure, we can see that both CM curves have similar shapes and there exists a steady error in between. This is due to the inertial parameter differences between A_G and A_G^{ref}, which also causes the initial value difference in h_G^{ref} and h_G at the beginning of a step. Having a steady error could consistently enable tracking action for the human-exoskeleton model. Additionally, Table I shows that assistive modes ($k_i < 1$)/resistive modes ($k_i > 1$) result in smaller/larger linear step velocities, which is reasonable since the reference CM that the human-exoskeleton model tracks is defined based on reduced/increased inertial parameters.

Metabolic costs using metrics (17) and (18) with different combinations of K_p and k_i are shown in Fig. 6, where the

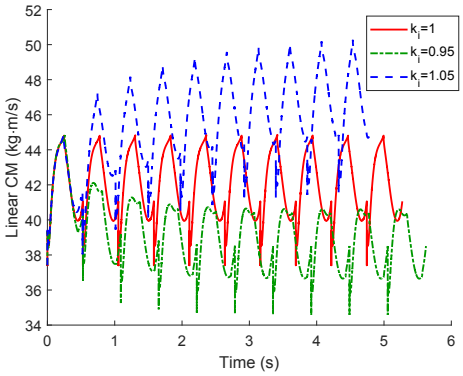

Fig. 4. Linear component of the biped's CM along the x-axis with different values of k_i and $K_p = 10 \cdot I_{6\times6}$. The blue ($k_i = 0.95$), red ($k_i = 1$), and green ($k_i = 1.05$) curves indicate assistive, passive, and resistive modes.

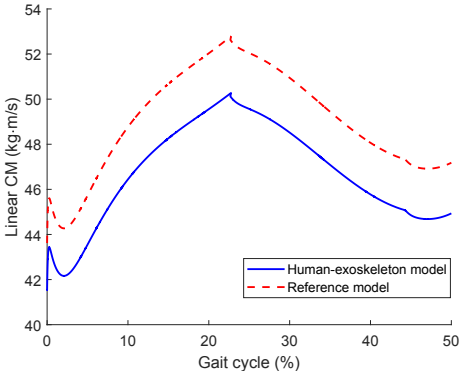

Fig. 5. Comparison of human-exoskeleton and reference model's linear CM along x-axis with $k_i = 1.05$ and $K_p = 10 \cdot I_{6\times6}$ over one steady step.

TABLE I

LINEAR STEP VELOCITY WITH $K_p = 10 \cdot I_{6\times6}$ & DIFFERENT VALUES OF k_i

k_i	Linear Step Velocity ($\text{m}\cdot\text{s}^{-1}$)
0.9	0.8332
0.95	0.9283
1	1.0113
1.03	1.0661
1.05	1.1172

black dotted line ($k_i = 1$) indicates the cost of the passive gait across different values of K_p. For a fixed K_p, the estimated metabolic cost increases almost proportionally with k_i. This result concurs with the expectation that increasing inertial parameters will result in more energy expenditure as the reference model represents a heavier person. The opposite conclusion can be drawn for the assistive case, i.e., reduced inertial parameters results in less energy expenditure during walking. Furthermore, for each given k_i, increasing K_p shows a trend of intensifying the performance of the proposed shaping strategy, i.e., a larger value of K_p yields more metabolic cost reduction (assistive mode) or increment (resistive mode). This is rational since a larger value of K_p generates a greater difference $h_G - h_G^{\text{ref}}$ in (6), which consequently leads to greater tracking action. Based on the biped model used in the paper, we can increase/decrease the metabolic cost by 18% and 36%, respectively, after which there is excessive/insufficient energy for the biped to maintain

a stable walking gait.

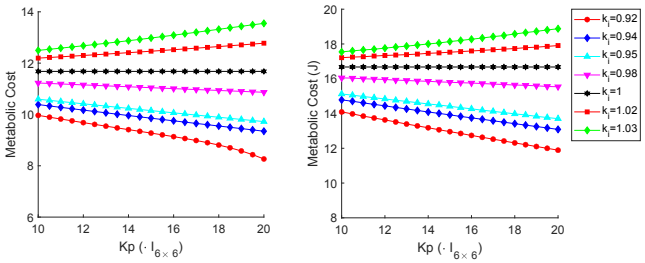

Fig. 6. Metabolic cost with different combinations of K_p and k_i using metrics (17) (left) and (18) (right).

The exoskeleton's torques during one steady step are shown in Fig. 7, which are bounded and smooth except during transitions. Discontinuities in the torques are due to the sudden changes in joint velocities during impacts. Also, the directions (extension/flexion) of the hip and knee torques roughly align with human joint torques [38], which is beneficial for human walking. Since we solved the shaping law in a lower-dimensional space, the result to (11) will guarantee the biped to track the desired CM, while the joint level-torques were left to be unspecified. This may be the cause for the misalignment between the exoskeleton stance knee torque and human knee torque during 0s to 0.1s. Possible ways to specify the joint-level torque would be adjusting the weight matrix W in (11) and incorporating constraints on specific actuators.

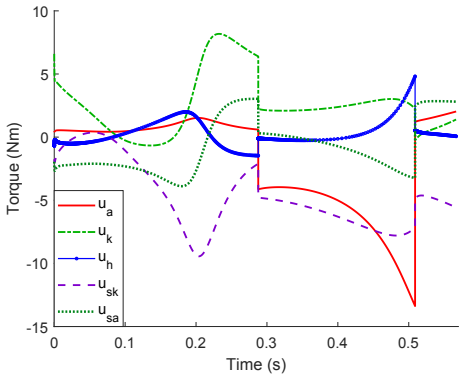

Fig. 7. Exoskeleton torques with $k_i = 0.95$ and $K_p = 10 \cdot I_{6\times 6}$ during one steady step.

The NDO is mainly designed for estimating human joint torques in experiments, while in simulation we can obtain τ_{hum} directly from the simulator instead of using the NDO. The estimation performance of the proposed NDO during passive walking is shown in Fig. 8, where we chose L with identical diagonal elements. We can see that for all choices of L, the 2-norm of the error term $||e||_2$ converges relatively fast and remains bounded after a short period of time. Note that if the L is chosen large enough, e.g., $L = 10^6 \cdot I_{8\times 8}$, the error in the figure could be sufficiently small (less than 0.05) for estimating human inputs. The large initial estimation error in Fig. 8 is closely related to the initial value of $\hat{z}$. We can mitigate this error by taking advantage of nominal human torque values from previous studies [38].

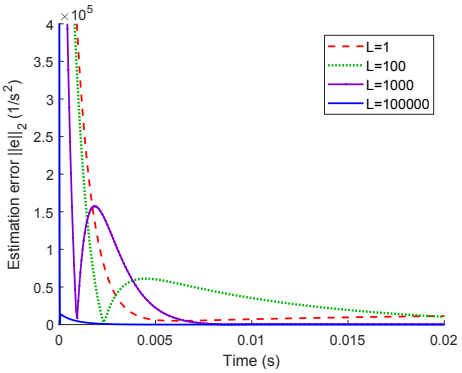

Fig. 8. Estimation error $||e||_2$ for $M^{-1}\tau_{\text{hum}}$ with different options of L.

D. Hybrid Stability

In this paper, biped locomotion is modeled as a dynamical system that includes continuous and discrete dynamics. Due to the difficulty of analytically proving the stability for high-dimensional hybrid systems in general, we verified the system's stability numerically using Poincaré sections method [30]. Let $x = (q^T, \dot{q}^T)^T$ denote the state vector of the biped, the transition from one step to the successive step can be modeled as a Poincaré map $\mathcal{P} : \mathcal{S} \to \mathcal{S}$, where $\mathcal{S}$ is the switching surface indicating initial heel contact. For a periodic orbit, its intersection with the switching surface is a fixed point x^*. The periodic orbit in the hybrid system is locally exponentially stable if the eigenvalues of the linearized Jacobian $\nabla_x \mathcal{P}(x^*)$ lie within the unit circle [30]. During simulation, we allowed the biped to converge to a fixed point with a specific set of shaping parameters and then numerically calculated the Jacobian eigenvalues using the perturbation analysis in [29]. Table II shows the maximum absolute eigenvalues of the linearized Poincaré map with different combinations of K_p and k_i. For most combinations in Table II, the hybrid system is stable. We will further investigate the relationship between shaping parameters and system stability in future work.

TABLE II
MAXIMUM EIGENVALUES OF THE LINEARIZED POINCARÉ MAP

K_p \ k_i	10	11	12	13	14	15	16
0.9	0.52	0.59	0.68	0.84	1.47	4.64	18.70
0.93	0.39	0.41	0.45	0.49	0.54	0.59	0.64
0.96	0.44	0.43	0.42	0.41	0.40	0.40	0.39
0.99	0.49	0.48	0.48	0.48	0.48	0.47	0.47
1.02	0.58	0.59	0.61	0.62	0.63	0.64	0.65

V. CONCLUSIONS

In this paper, we proposed a task-invariant shaping framework for lower-limb exoskeletons to assist/resist human users by altering the magnitude of their CM. The framework achieved the task-invariant objective by tracking a desired CM generated by a virtual reference model based on each individual's self-selected gaits. The fixed dimension of the CM vector guarantees the existence of a shaping law if the exoskeleton has at least three actuators. We incorporated an NDO to estimate human joint torques and applied an

optimization procedure to determine the shaping law with minimal control actions. Simulation results on a human-like biped demonstrated that the proposed strategy successfully altered the biped's CM and reduced (assistive mode) or increased (resistive mode) the estimated metabolic costs with different combinations of shaping parameters. Future work includes human subject experiments, alternative ways to define the desired CM, and customizing shaping parameters for optimal performance.

ACKNOWLEDGMENT

The authors thank Brook Schmid for her help on the simulation studies and editorial assistance.

REFERENCES

[1] T. Rantanen and J. Avela, "Leg extension power and walking speed in very old people living independently," *J. Gerontol. A Biol. Sci. Med. Sci.*, vol. 52, no. 4, pp. M225–M231, 1997.

[2] M. Frey, G. Colombo, M. Vaglio, R. Bucher, M. Jorg, and R. Riener, "A novel mechatronic body weight support system," *IEEE Trans. Neural Syst. Rehabil. Eng.*, vol. 14, no. 3, pp. 311–321, 2006.

[3] D. Ferris, G. Sawicki, and A. Domingo, "Powered lower limb orthoses for gait rehabilitation," *Top. Spinal Cord Inj. Rehabil.*, vol. 11, no. 2, pp. 34–49, 2005.

[4] C. Nave, Y. Yang, V. Viegas, and O. Postolache, "Physical rehabilitation based on smart walker," in *Int. Conf. Sens. Technol.*, Dec. 2018, pp. 388–393.

[5] A. J. Young and D. P. Ferris, "State of the art and future directions for lower limb robotic exoskeletons," *IEEE Trans. Neural Syst. Rehabil. Eng.*, vol. 25, no. 2, pp. 171–182, 2016.

[6] D. J. Hyun, H. Park, T. Ha, S. Park, and K. Jung, "Biomechanical design of an agile, electricity-powered lower-limb exoskeleton for weight-bearing assistance," *Robot. Auton. Syst.*, vol. 95, pp. 181–195, 2017.

[7] L. M. Mooney, E. J. Rouse, and H. M. Herr, "Autonomous exoskeleton reduces metabolic cost of human walking during load carriage," *J. NeuroEng. Rehabil.*, vol. 11, no. 1, pp. 1–11, 2014.

[8] T. Yan, M. Cempini, C. M. Oddo, and N. Vitiello, "Review of assistive strategies in powered lower-limb orthoses and exoskeletons," *Robot. Auton. Syst.*, vol. 64, pp. 120–136, 2015.

[9] H. Quintero, R. Farris, C. Hartigan, I. Clesson, and M. Goldfarb, "A powered lower limb orthosis for providing legged mobility in paraplegic individuals," *Top. Spinal Cord Inj. Rehabil.*, vol. 17, no. 1, pp. 25–33, 2011.

[10] D. Sanz-Merodio, M. Cestari, J. C. Arevalo, and E. Garcia, "Control motion approach of a lower limb orthosis to reduce energy consumption," *Int. J. Adv. Robot. Syst.*, vol. 9, no. 6, p. 232, 2012.

[11] M. K. Shepherd and E. J. Rouse, "Design and validation of a torque-controllable knee exoskeleton for sit-to-stand assistance," *IEEE/ASME Trans. Mechatron.*, vol. 22, no. 4, pp. 1695–1704, 2017.

[12] W. Ma, H. Cheng, R. Huang, and Q. Chen, "Gait planning with dynamic movement primitives for lower limb exoskeleton walking up stairs," in *IEEE Int. Conf. Robot. Biomim*, Dec. 2018, pp. 703–708.

[13] S. Wang, L. Wang, C. Meijneke, E. Van Asseldonk, T. Hoellinger, G. Cheron, Y. Ivanenko, V. La Scaleia, F. Sylos-Labini, M. Molinari *et al.*, "Design and control of the mindwalker exoskeleton," *IEEE Trans. Neural Syst. Rehabil. Eng.*, vol. 23, no. 2, pp. 277–286, 2014.

[14] L. Wang, S. Wang, E. H. van Asseldonk, and H. van der Kooij, "Actively controlled lateral gait assistance in a lower limb exoskeleton," in *IEEE Int. Conf. Intell. Robots Syst.*, Nov. 2013, pp. 965–970.

[15] S. Y. Gordleeva, S. A. Lobov, N. A. Grigorev, A. O. Savosenkov, M. O. Shamshin, M. V. Lukoyanov, M. A. Khoruzhko, and V. B. Kazantsev, "Real-time EEG–EMG human–machine interface-based control system for a lower-limb exoskeleton," *IEEE Access*, vol. 8, pp. 84 070–84 081, 2020.

[16] G. Lv and R. D. Gregg, "Underactuated potential energy shaping with contact constraints: Application to a powered knee-ankle orthosis," *IEEE Trans. Control Syst. Technol.*, vol. 26, no. 1, pp. 181–193, 2017.

[17] J. Lin, G. Lv, and R. D. Gregg, "Contact-invariant total energy shaping control for powered exoskeletons," in *Am. Control Conf.* IEEE, 2019, pp. 664–670.

[18] J. Lin, N. V. Divekar, G. Lv, and R. D. Gregg, "Optimal task-invariant energetic control for a knee-ankle exoskeleton," *IEEE Control Systems Letters*, vol. 5, no. 5, pp. 1711–1716, 2020.

[19] G. C. Thomas and R. D. Gregg, "An energy shaping exoskeleton controller for human strength amplification," in *Proc. IEEE 58th Conf. Decis. Control*, Dec. 2021, pp. 1419–1425.

[20] D. E. Orin, A. Goswami, and S.-H. Lee, "Centroidal dynamics of a humanoid robot," *Auton. robots*, vol. 35, no. 2, pp. 161–176, 2013.

[21] J. H. Jung, L. V. Opheusden, P. Barralon, and J. F. Veneman, "Real time computation of centroidal momentum for the use as a stability index applicable to human walking with exoskeleton," in *Wearable Robotics: Challenges and Trends*. Springer, 2017, pp. 157–161.

[22] C. Bayon, A. Emmens, M. Afschrift, T. Van Wouwe, A. Keemink, H. Van Der Kooij, and E. Van Asseldonk, "Can momentum-based control predict human balance recovery strategies?" *IEEE Trans. Neural Syst. Rehabil. Eng.*, vol. 28, no. 9, pp. 2015–2024, 2020.

[23] G. Patil, L. Rigoli, M. J. Richardson, M. Kumar, and T. Lorenz, "Momentum-based trajectory planning for lower-limb exoskeletons supporting sit-to-stand transitions," *Int. J. Intell. Robot. Appl.*, vol. 2, no. 2, pp. 180–192, 2018.

[24] T. Koolen, S. Bertrand, G. Thomas, T. De Boer, T. Wu, J. Smith, J. Englsberger, and J. Pratt, "Design of a momentum-based control framework and application to the humanoid robot atlas," *Int. J. Humanoid Robot.*, vol. 13, no. 01, p. 1650007, 2016.

[25] M. Liu, D. Qu, F. Xu, F. Zou, P. Di, and C. Tang, "Quadrupedal robots whole-body motion control based on centroidal momentum dynamics," *Applied Sciences*, vol. 9, no. 7, p. 1335, 2019.

[26] T. A. Johansen, T. I. Fossen, and P. Tøndel, "Efficient optimal constrained control allocation via multiparametric programming," *J. Guid. Control Dyn.*, vol. 28, no. 3, pp. 506–515, 2005.

[27] M. Q. Liu, F. C. Anderson, M. G. Pandy, and S. L. Delp, "Muscles that support the body also modulate forward progression during walking," *J. Biomech.*, vol. 39, no. 14, pp. 2623–2630, 2006.

[28] R. M. Murray, Z. Li, and S. S. Sastry, *A mathematical introduction to robotic manipulation*. NW Boca Raton, FL: CRC press, 2017.

[29] G. Lv, H. Zhu, and R. D. Gregg, "On the design and control of highly backdrivable lower-limb exoskeletons: A discussion of past and ongoing work," *IEEE Control Syst. Mag.*, vol. 38, no. 6, pp. 88–113, 2018.

[30] E. R. Westervelt, J. W. Grizzle, C. Chevallereau, J. H. Choi, and B. Morris, *Feedback control of dynamic bipedal robot locomotion*. NW Boca Raton, FL: CRC press, 2018.

[31] W.-H. Chen, D. J. Ballance, P. J. Gawthrop, and J. O'Reilly, "A nonlinear disturbance observer for robotic manipulators," *IEEE Trans. Ind. Electron.*, vol. 47, no. 4, pp. 932–938, 2000.

[32] H. K. Khalil, *Nonlinear systems; 3rd ed.* Upper Saddle River, NJ: Prentice-Hall, 2002.

[33] P. Johan From, I. Schjølberg, J. Tommy Gravdahl, K. Ytterstad Pettersen, and T. I. Fossen, "On the boundedness property of the inertia matrix and skew-symmetric property of the coriolis matrix for vehicle-manipulator systems," *J. Syst., Meas., Control*, vol. 134, no. 4, p. 044501, 2012.

[34] G. Williams, B. F. Mentiplay, M. B. Kahn, R. A. Clark, and M. Banky, "The effect of walking speed on lower limb angular velocity," *Arch. Phys. Med. Rehabil.*, vol. 99, no. 10, pp. e12–e13, 2018.

[35] G. Lv, J. Lin, and R. D. Gregg, "Trajectory-free control of lower-limb exoskeletons through underactuated total energy shaping," *IEEE Access*, vol. 9, pp. 95 427–95 443, 2021.

[36] A. Martin and J. Schmiedeler, "Predicting human walking gaits with a simple planar model," *J. Biomech.*, vol. 47, no. 6, pp. 1416–1421, 2014.

[37] S. Faraji, A. R. Wu, and A. J. Ijspeert, "A simple model of mechanical effects to estimate metabolic cost of human walking," *Sci. Rep.*, vol. 8, no. 1, pp. 1–12, 2018.

[38] D. A. Winter, *Biomechanics and motor control of human movement*. John Wiley & Sons, 2009.